Supplement of Atmos. Chem. Phys., 22, 9663–9680, 2022
https://doi.org/10.5194/acp-22-9663-2022-supplement

Atmospheric Chemistry and Physics
Open Access
EGU

Supplement of

The ice-nucleating activity of African mineral dust in the Caribbean boundary layer

Alexander D. Harrison et al.

Correspondence to: Benjamin J. Murray (b.j.murray@leeds.ac.uk)

–

Contents of this file

Text S1: Background subtraction and error calculations.

Table S1: Sampling durations and the volume of air sampled for 28 samples collected onto filters and their corresponding symbols used in Figure 2a. Aerosol surface areas were only calculated for filters where both SMPS and APS measurements were available.

Figures S1 to S9

Text S1. Background subtraction and error calculations

The microlitre Nucleation by Immersed Particle Instrument (µL-NIPI) droplet freezing assay has been described previously (Whale et al., 2015). Briefly, this technique involves pipetting an array of 1 µl droplets onto a hydrophobic surface and cooling them at a defined rate (1 °C min^{-1}). A camera allows the user to determine when each droplet freezes and relate this to the droplet freezing temperature via synchronised temperature measurements. In this technique, droplets of ultrapure water (not containing aerosol) always freeze well above that expected for homogeneous freezing, indicating that there are contaminants in both the water and on the substrate. When the atmospheric INP concentration is relatively low, the fraction frozen curves for the handling blanks (where water has been exposed to the same process as when a sample is involved) is very close to or sometimes indistinguishable from the fraction frozen curve for an aerosol sample. Hence, it is necessary to background subtract the data and appropriately account for the uncertainties.

While ice nucleation data is often reported in cumulative quantities, such as fraction frozen or INP concentration, it is necessary to do the background subtraction with the differential quantity. That is, we need to do the subtraction with a quantity where we have nucleation events expressed per temperature interval (Vali, 2019).

To determine the contribution of impurities to the overall INP signal of the collected aerosol samples during µL-NIPI analysis, we first collated all of the blanks and handling blanks into a single dataset and produced a polynomial fit to represent the baseline. This was achieved by binning all of the droplet freezing assay data for the individual blank runs into 0.5 °C temperature intervals and calculating the differential nucleus spectrum, $k(T)$, in terms of freezing events per unit volume per degree Celsius, using Equation 1:

$$k(T) = -\frac{1}{v \cdot \Delta T} \cdot \ln\left(1 - \frac{\Delta N(T)}{N(T)}\right) \qquad \text{Equation 1}$$

where v is the volume of the droplets used (1 µL), ΔT is the temperature interval (0.5 °C), ΔN is the number of droplets that froze in the temperature interval and $N(T)$ is the total number of droplets.

The first set of temperature intervals, in which freezing events occurred but were separated from the bulk of the data by more than 1 °C, were removed from the overall compilation of the baseline data since these data points had very large Poisson uncertainties. Once compiled, a polynomial fit was applied to the data and the standard deviation was calculated. The background $k(T)$ was approximated by $\log k(T) = -1.57 \times 10^{-2}\, T^2 - 9.46T - 11.22$, with a standard deviation of ± 0.3 cm^{-3} $°C^{-1}$ (see Figure S1).

The freezing data for the aerosol samples was then also binned into 0.5°C intervals and $k(T)$ determined along with uncertainties. If a data point (with associated error) was consistent with the background, then this was then regarded as an upper limit. Figure S2 shows two examples, one example falls completely within the baseline and one example only has a few points above that are limiting. In Figure S3, we show the background-subtracted values of $k(T)$ where background values (using the parameterisation) were subtracted from those for the aerosol samples. Limiting values are indicated as open symbols. The uncertainty associated with the background was determined using the uncertainty range in the background. This uncertainty was combined with the Poisson uncertainty in quadrature.

These errors were then converted into the cumulative quantity (i.e. the integrated volume density of active sites), $K(T)$, by summing $k(T)$ for all temperatures greater than T (see Figure S3) (Vali, 2019).

This allowed for the errors to be calculated in other cumulative expressions such as INP concentration ([INP]) and $n_s(T)$. When plotting the cumulative plots in Figure 2 and Figure 3, the data points which are consistent with zero (i.e. are upper limits) are shown as hollow symbols. This is common for the first few data points in a spectrum, but in some cases the whole spectrum was in the baseline. In the case where $k(T)$ is equal to or smaller than the background value, but where $k(T)$ at higher temperatures is positive, the best estimate does not increase at those temperatures. For example, the $k(T)$ values at -25.75 °C, -26.25 °C and -26.75 °C in Figure S2b for sample '170819_1116_1606' are all below the best fit background line. In Figure S3, the best estimate of $K(T)$ does not increase at these temperatures. If $k(T)$ at any higher T was above the baseline (lower error bar above upper bound of the background), then all points below that T in $K(T)$ would have a lower bound above zero.

Supplementary Tables

Table S1: Sampling durations and the volume of air sampled for 28 samples collected onto filters and their corresponding symbols used in Figure 4. Aerosol surface areas were only calculated for filters where both SMPS and APS measurements were available.

Symbol	Start	End	Vol. Air sampled (Litres)	Aerosol surface area ($\mu m^2\ cm^{-3}$)
■	24/08/17 11:30	24/08/17 18:00	6513	30.2
■	19/08/17 16:15	19/08/17 18:44	2488	N/A
■	19/08/17 11:16	19/08/17 16:06	4843	N/A
■	17/08/17 15:43	17/08/17 18:31	2805	N/A
■	17/08/17 11:02	18/08/17 11:17	24299	N/A
■	16/08/17 20:31	17/08/17 05:15	8750	N/A
■	15/08/17 20:38	15/08/17 23:02	2405	35.9
■	15/08/17 15:40	15/08/17 23:24	7749	40.0
■	13/08/17 13:40	14/08/17 02:31	12876	11.3
■	13/08/17 16:34	13/08/17 17:41	1119	13.0
■	10/08/17 02:05	10/08/17 05:37	3540	N/A
■	09/08/17 18:56	10/08/17 05:46	10855	N/A
■	09/08/17 10:15	09/08/17 12:57	2705	N/A
■	04/08/17 18:42	05/08/17 10:16	15598	N/A
■	04/08/17 10:21	04/08/17 18:37	8283	N/A
■	04/08/17 10:07	04/08/17 18:40	8567	N/A
■	03/08/17 09:49	03/08/17 19:27	9653	12.5
■	02/08/17 14:32	02/08/17 16:50	2305	24.1
■	02/08/17 10:44	02/08/17 20:47	10070	26.4
■	02/08/17 10:43	02/08/17 14:28	3758	29.1
■	01/08/17 10:20	01/08/17 22:50	12525	32.8
■	31/07/17 16:22	01/08/17 06:42	14362	25.9
■	31/07/17 16:22	31/07/17 18:05	1720	21.1
■	31/07/17 09:09	31/07/17 16:19	7164	20.5
■	29/07/17 14:47	31/07/17 03:08	36423	16.0
■	27/07/17 12:05	28/07/17 09:41	21643	19.0
■	26/07/17 10:15	27/07/17 11:44	25534	N/A
■	24/07/17 08:31	24/07/17 16:17	7766	35.2

Supplementary Figures

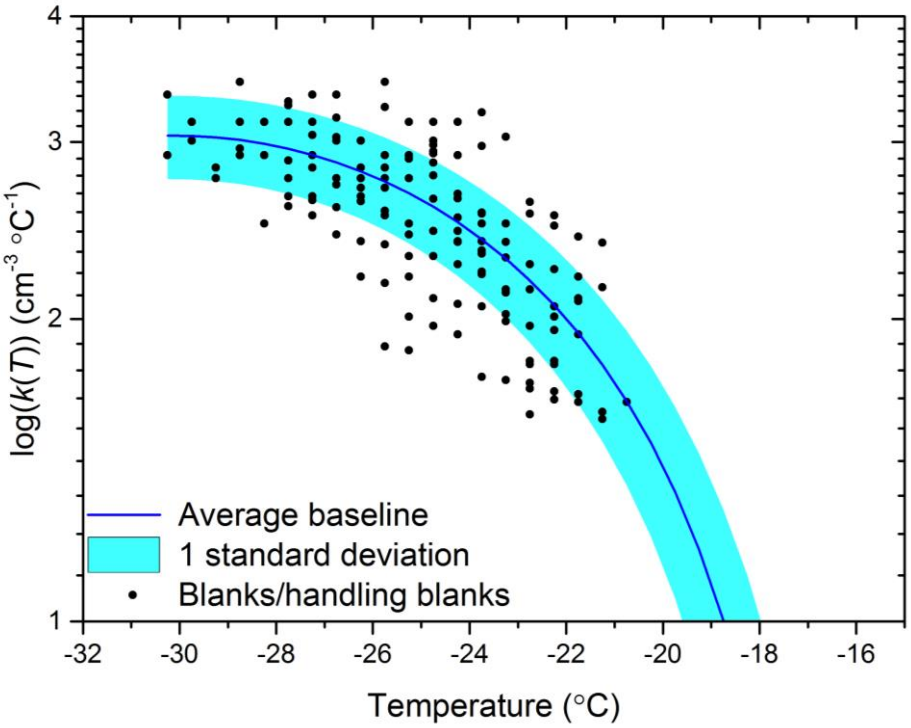

Figure S1: Plot of log $k(T)$, where $k(T)$ is the differential nucleus spectrum, versus temperature for the baselines of the experiments, together with the exponential fit and standard deviation used to represent the baseline in subsequent error calculations and background subtractions.

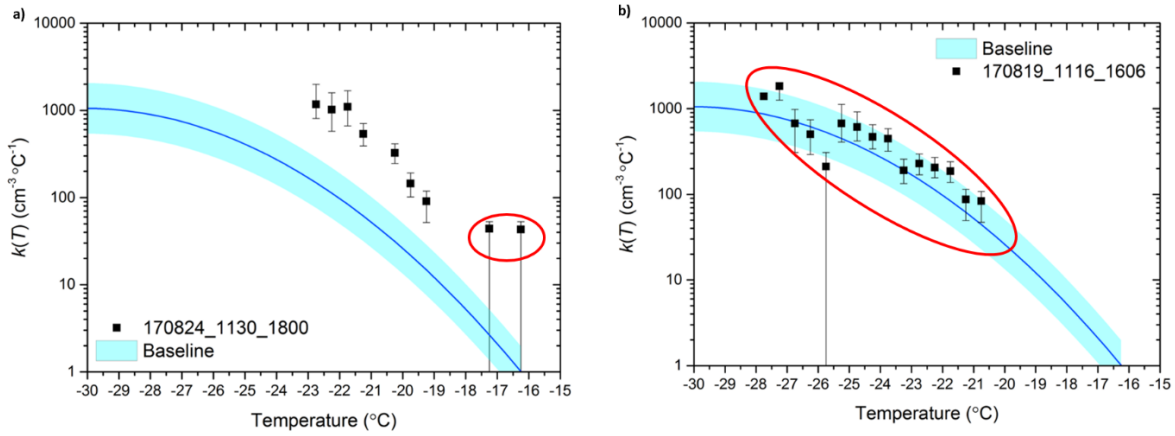

Figure S2: $k(T)$ versus temperature for two examples of collected aerosol. Also plotted is the representation of the baseline (background impurities) from Figure S1. Data points that are highlighted by a red oval are not considered to be statistically above the background signal; when later converted to cumulative quantities for $K(T)$, [INP] and $n_s(T)$ plots, these would be shown as hollow symbols to represent that they are considered to be upper limits. a) An example where the majority of the data points are above the baseline, and hence are statistically significant. The first two freezing events at the warmest temperatures (outlined by the red oval) have large uncertainties and so cannot be said to be statistically above the baseline. b) An example where the INP signal is not significantly above the background signal and so all data points are consistent with the baseline.

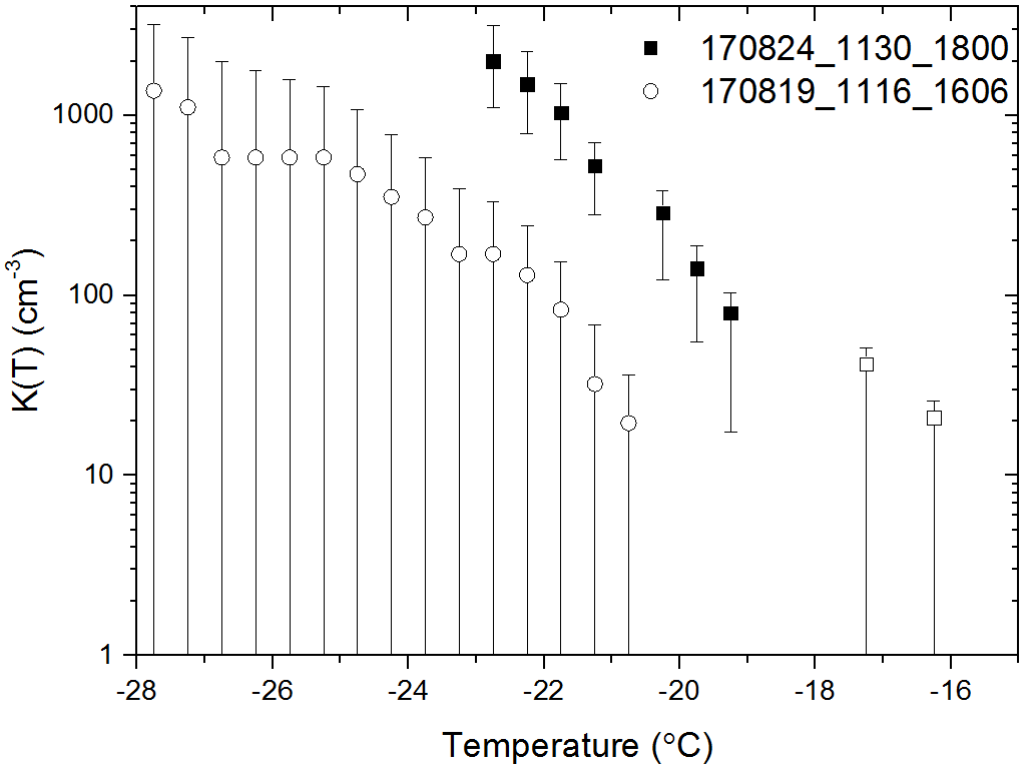

Figure S3: The calculated cumulative spectrum (or integrated volume density of active sites), $K(T)$, values for the examples from Figure S2 and their corresponding errors. Hollow symbols represent data points which are statistically within the baseline and so are considered to be upper values.

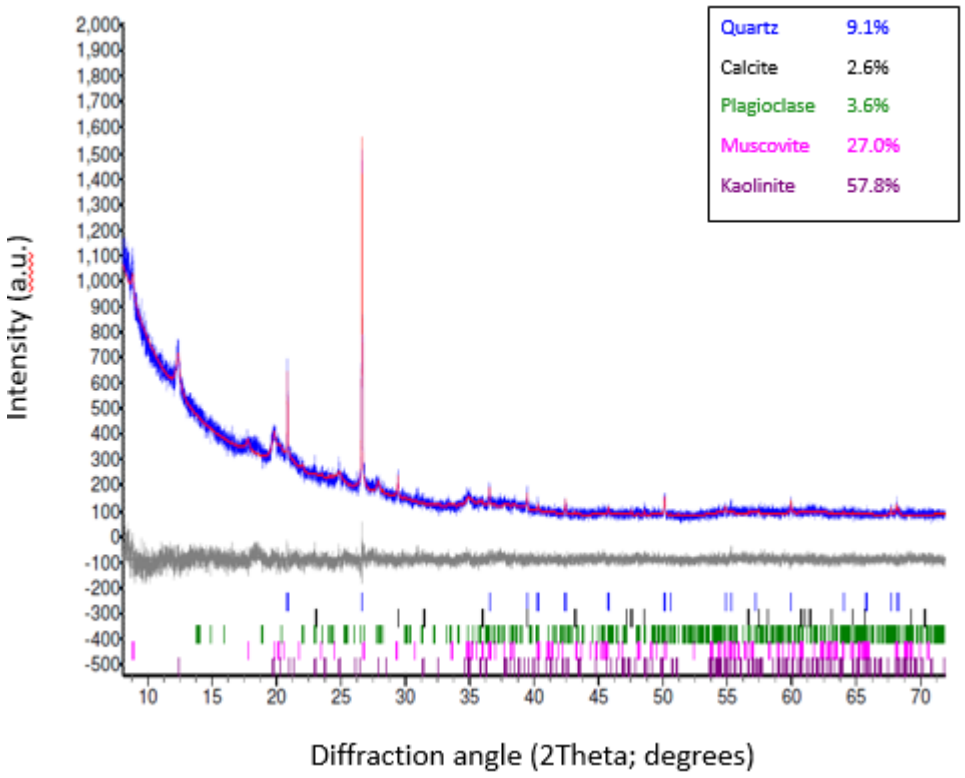

Figure S4: Powder X-ray diffraction analysis and Rietveld refinement of aerosol collected in rain water from the 3rd-4th of August 2017. The proportion of each mineral identified in the sample is shown in the key. The limit of detection of this technique was ~2 wt%, hence K-feldspar was below this limit, thus defining an upper limit. X-ray diffraction combined with Rietveld refinement analysis is a technique for quantifying the proportions of the crystalline components of a sample. Crystalline components have a set of sharp Bragg peaks that are characteristic of a particular crystalline material. The X-ray diffractometer (Bruker D8) was equipped with a source supplying X-rays at 1.54060 Å. The diffraction pattern is shown in blue, while the fitted Rietveld pattern (a combination of the patterns associated with a range of minerals) is shown in pink. The positions of the Bragg peaks are associated with each mineral are shown below the patterns and are colour coded according to the key. The grey line is the residual (i.e. the difference between the fitted and measured patterns.

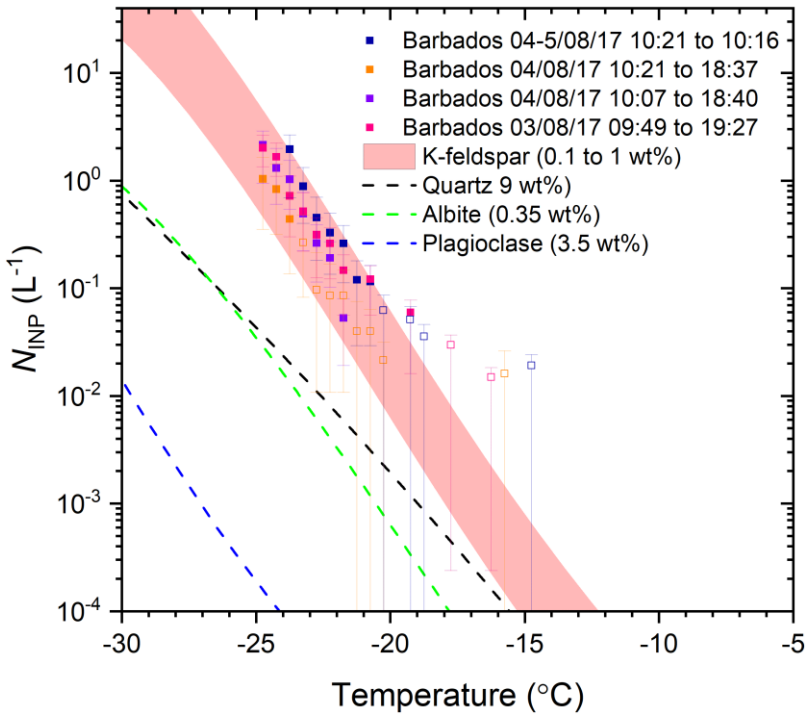

Figure S5: INP concentration predictions based on the mineralogy of the dust sample collected from rainwater and the 3rd and 4th August 2017. Parameterisations for from Harrison et al. (2019) were scaled according to the proportions determined by X-ray diffraction for quartz, albite and plagioclase and the estimated value from the SEM analysis for K-feldspar.

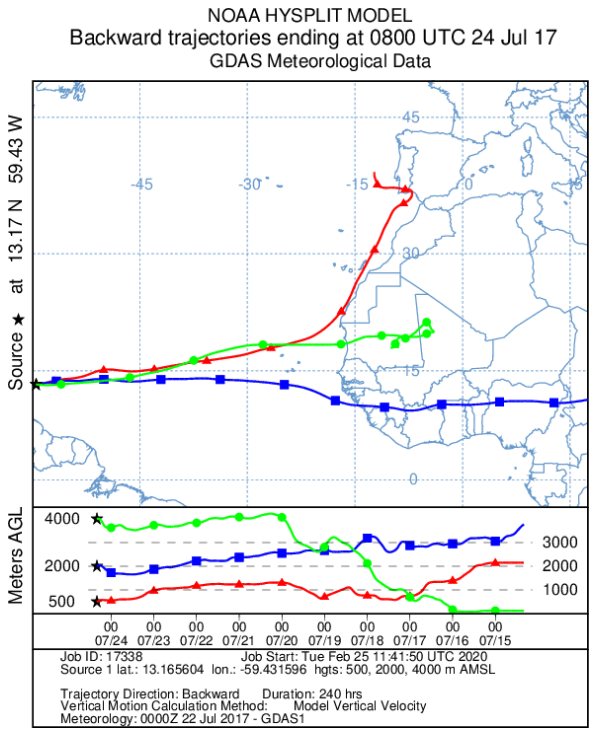
NOAA HYSPLIT MODEL
Backward trajectories ending at 0800 UTC 24 Jul 17
GDAS Meteorological Data
Source ★ at 13.17 N 59.43 W
Meters AGL
Job ID: 17338 Job Start: Tue Feb 25 11:41:50 UTC 2020
Source 1 lat.: 13.165604 lon.: -59.431596 hgts: 500, 2000, 4000 m AMSL
Trajectory Direction: Backward Duration: 240 hrs
Vertical Motion Calculation Method: Model Vertical Velocity
Meteorology: 0000Z 22 Jul 2017 - GDAS1

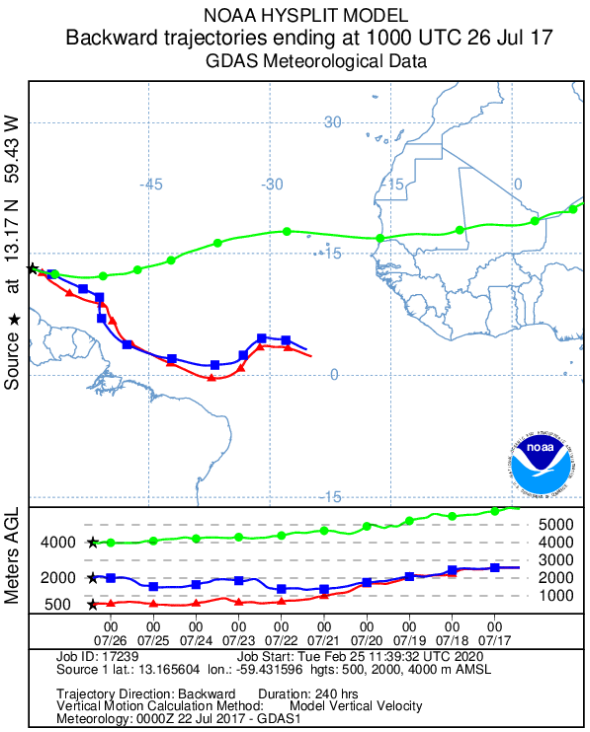
NOAA HYSPLIT MODEL
Backward trajectories ending at 1000 UTC 26 Jul 17
GDAS Meteorological Data
Source ★ at 13.17 N 59.43 W
Meters AGL
Job ID: 17239 Job Start: Tue Feb 25 11:39:32 UTC 2020
Source 1 lat.: 13.165604 lon.: -59.431596 hgts: 500, 2000, 4000 m AMSL
Trajectory Direction: Backward Duration: 240 hrs
Vertical Motion Calculation Method: Model Vertical Velocity
Meteorology: 0000Z 22 Jul 2017 - GDAS1

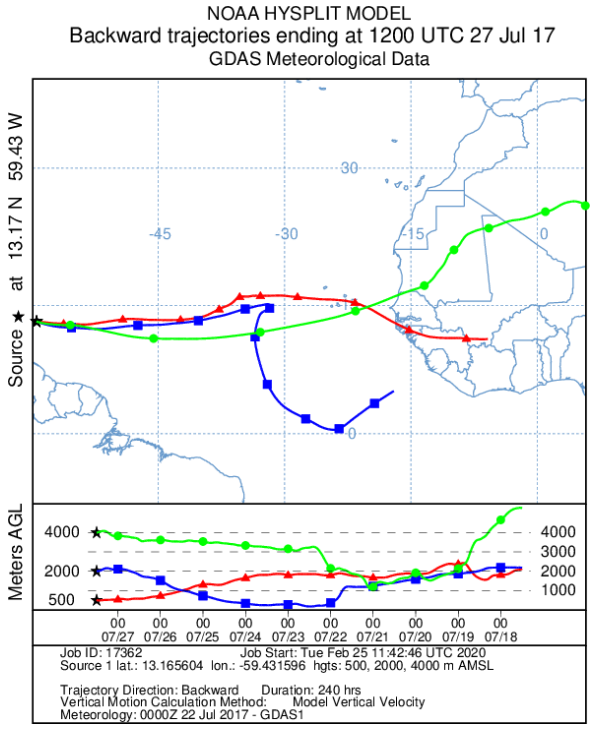
NOAA HYSPLIT MODEL
Backward trajectories ending at 1200 UTC 27 Jul 17
GDAS Meteorological Data
Source ★ at 13.17 N 59.43 W
Meters AGL
Job ID: 17362 Job Start: Tue Feb 25 11:42:46 UTC 2020
Source 1 lat.: 13.165604 lon.: -59.431596 hgts: 500, 2000, 4000 m AMSL
Trajectory Direction: Backward Duration: 240 hrs
Vertical Motion Calculation Method: Model Vertical Velocity
Meteorology: 0000Z 22 Jul 2017 - GDAS1

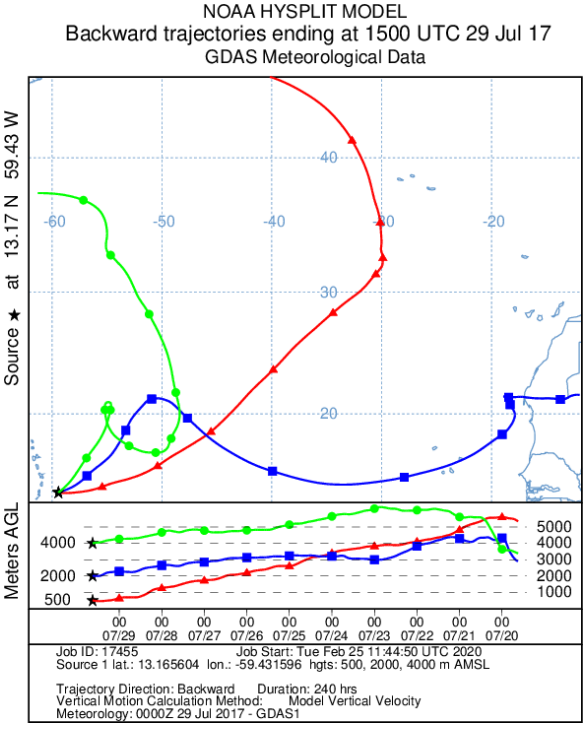
NOAA HYSPLIT MODEL
Backward trajectories ending at 1500 UTC 29 Jul 17
GDAS Meteorological Data
Source ★ at 13.17 N 59.43 W
Meters AGL
Job ID: 17455 Job Start: Tue Feb 25 11:44:50 UTC 2020
Source 1 lat.: 13.165604 lon.: -59.431596 hgts: 500, 2000, 4000 m AMSL
Trajectory Direction: Backward Duration: 240 hrs
Vertical Motion Calculation Method: Model Vertical Velocity
Meteorology: 0000Z 29 Jul 2017 - GDAS1

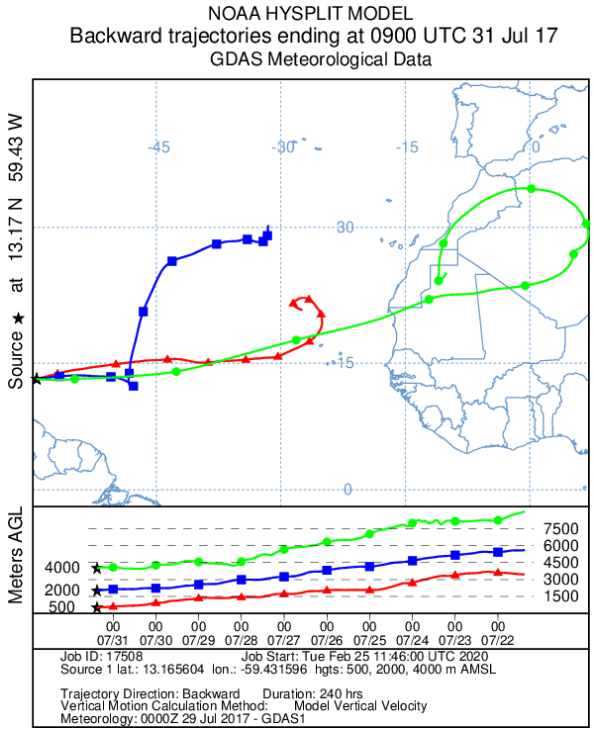
NOAA HYSPLIT MODEL
Backward trajectories ending at 0900 UTC 31 Jul 17
GDAS Meteorological Data
Source ★ at 13.17 N 59.43 W
Meters AGL
Job ID: 17508 Job Start: Tue Feb 25 11:46:00 UTC 2020
Source 1 lat.: 13.165604 lon.: -59.431596 hgts: 500, 2000, 4000 m AMSL
Trajectory Direction: Backward Duration: 240 hrs
Vertical Motion Calculation Method: Model Vertical Velocity
Meteorology: 0000Z 29 Jul 2017 - GDAS1

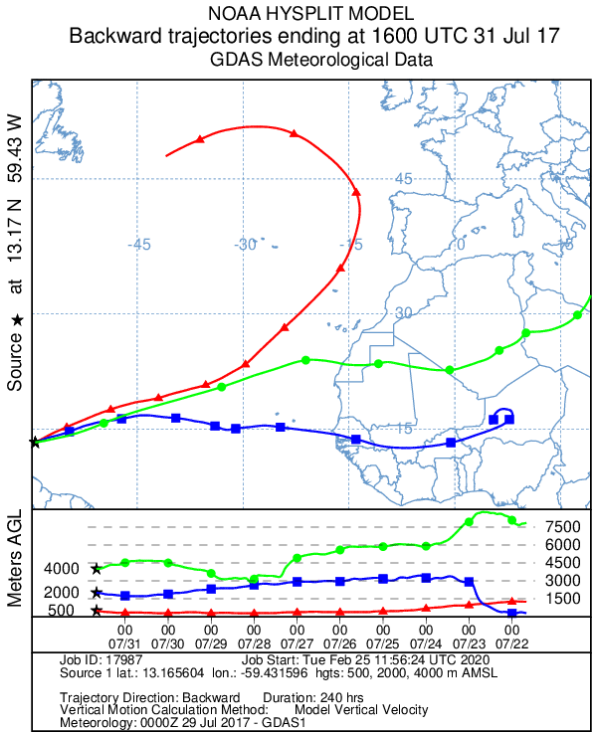
NOAA HYSPLIT MODEL
Backward trajectories ending at 1600 UTC 31 Jul 17
GDAS Meteorological Data
Source ★ at 13.17 N 59.43 W
Meters AGL
Job ID: 17987 Job Start: Tue Feb 25 11:56:24 UTC 2020
Source 1 lat.: 13.165604 lon.: -59.431596 hgts: 500, 2000, 4000 m AMSL
Trajectory Direction: Backward Duration: 240 hrs
Vertical Motion Calculation Method: Model Vertical Velocity
Meteorology: 0000Z 29 Jul 2017 - GDAS1

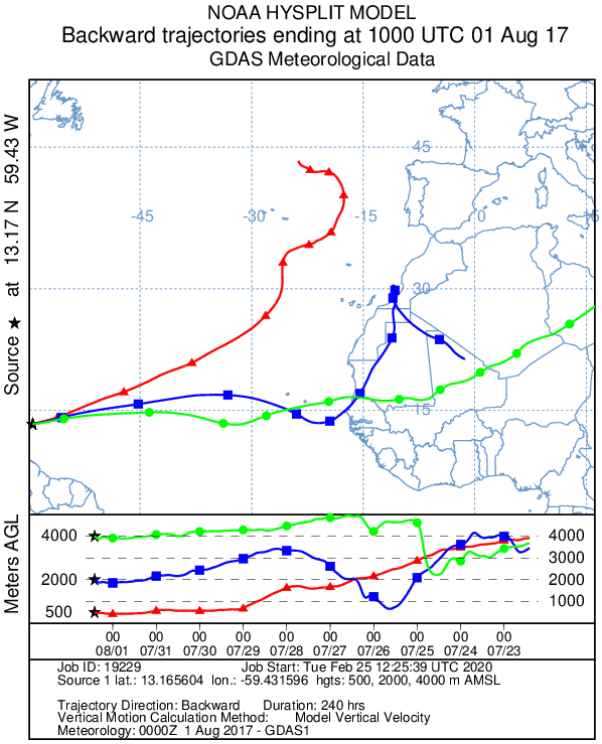
NOAA HYSPLIT MODEL
Backward trajectories ending at 1000 UTC 01 Aug 17
GDAS Meteorological Data
Source ★ at 13.17 N 59.43 W
Meters AGL
Job ID: 19229 Job Start: Tue Feb 25 12:25:39 UTC 2020
Source 1 lat.: 13.165604 lon.: -59.431596 hgts: 500, 2000, 4000 m AMSL
Trajectory Direction: Backward Duration: 240 hrs
Vertical Motion Calculation Method: Model Vertical Velocity
Meteorology: 0000Z 1 Aug 2017 - GDAS1

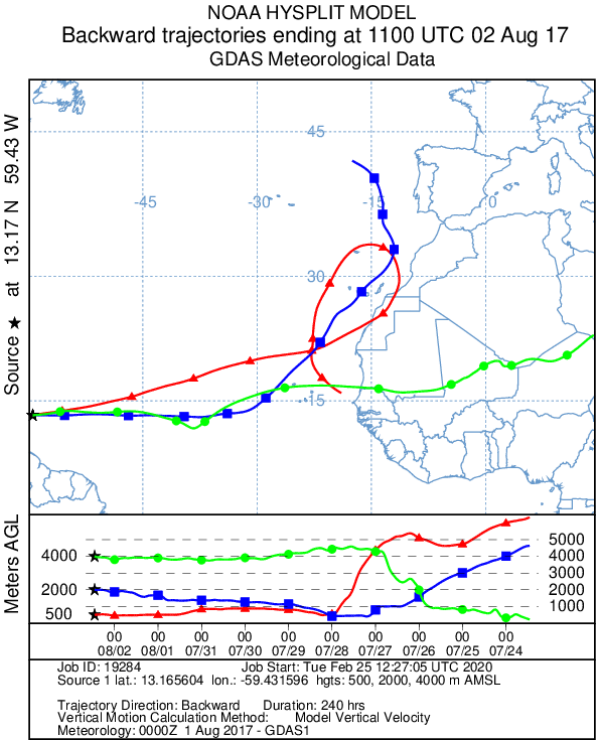
NOAA HYSPLIT MODEL
Backward trajectories ending at 1100 UTC 02 Aug 17
GDAS Meteorological Data
Source ★ at 13.17 N 59.43 W
Meters AGL
Job ID: 19284 Job Start: Tue Feb 25 12:27:05 UTC 2020
Source 1 lat.: 13.165604 lon.: -59.431596 hgts: 500, 2000, 4000 m AMSL
Trajectory Direction: Backward Duration: 240 hrs
Vertical Motion Calculation Method: Model Vertical Velocity
Meteorology: 0000Z 1 Aug 2017 - GDAS1

NOAA HYSPLIT MODEL
Backward trajectories ending at 1500 UTC 02 Aug 17
GDAS Meteorological Data

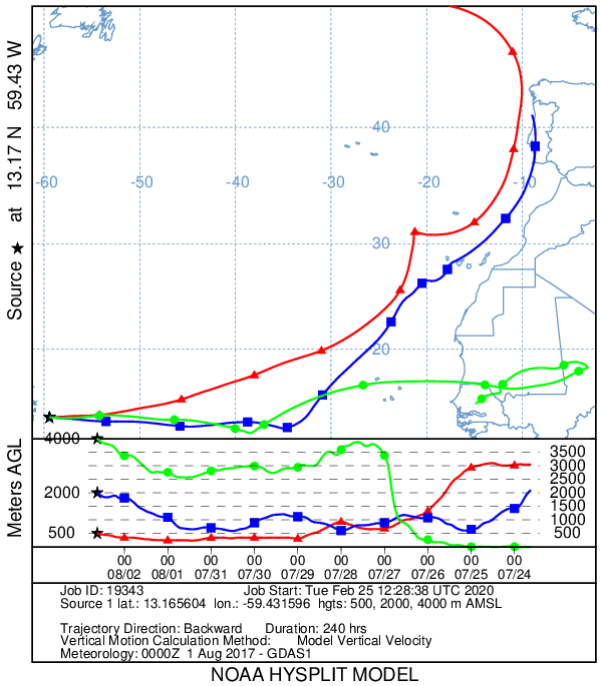

NOAA HYSPLIT MODEL
Backward trajectories ending at 1000 UTC 03 Aug 17
GDAS Meteorological Data

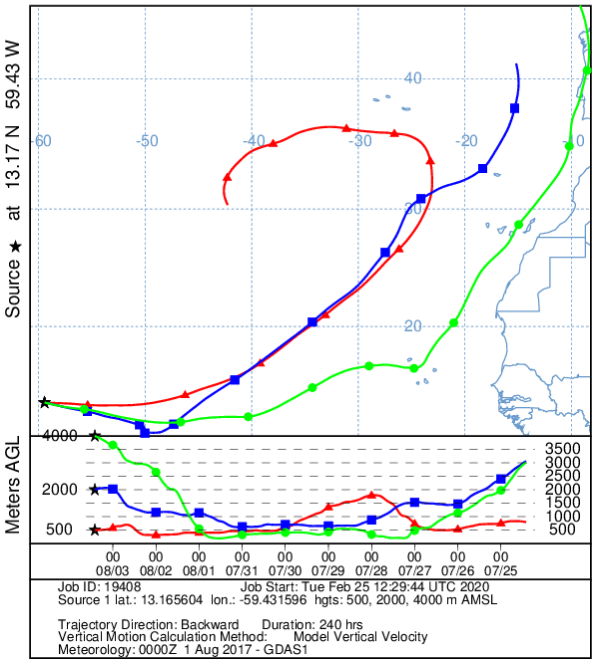

NOAA HYSPLIT MODEL
Backward trajectories ending at 1000 UTC 04 Aug 17
GDAS Meteorological Data

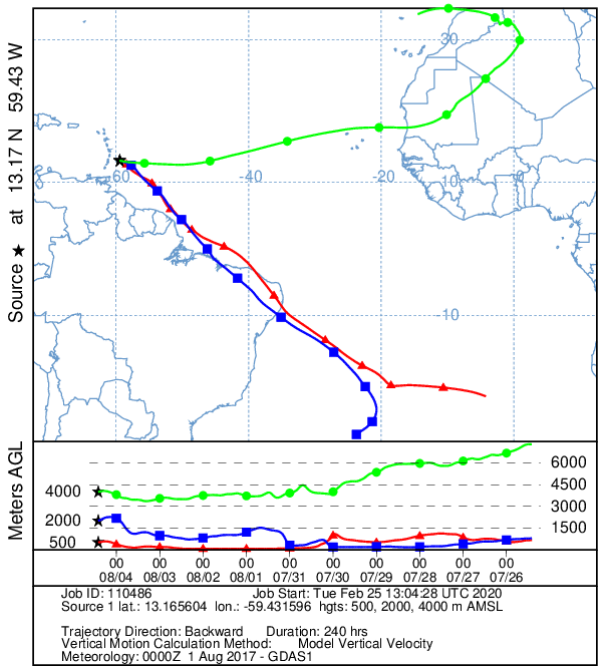

NOAA HYSPLIT MODEL
Backward trajectories ending at 1900 UTC 04 Aug 17
GDAS Meteorological Data

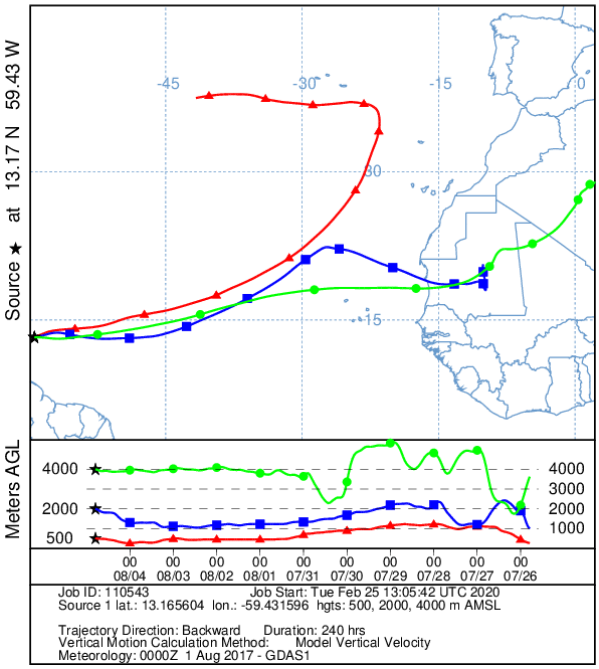

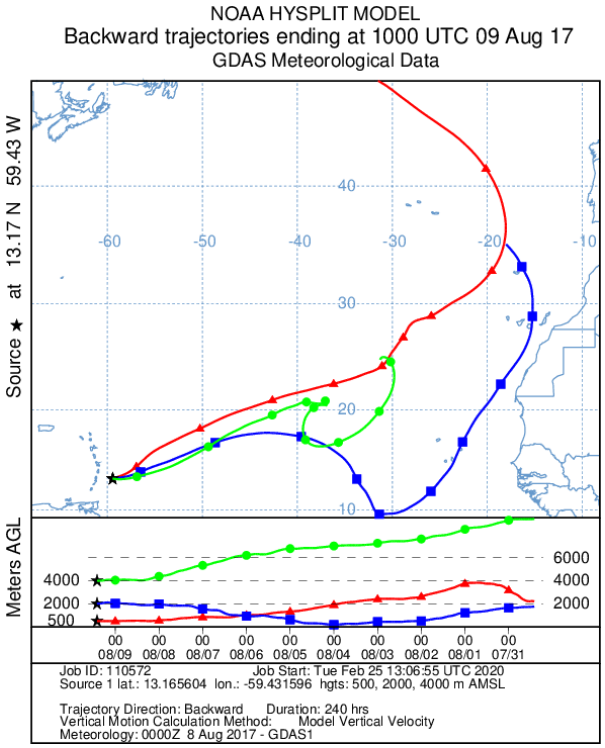
NOAA HYSPLIT MODEL
Backward trajectories ending at 1000 UTC 09 Aug 17
GDAS Meteorological Data
Source ★ at 13.17 N 59.43 W
Meters AGL
Job ID: 110572 Job Start: Tue Feb 25 13:06:55 UTC 2020
Source 1 lat.: 13.165604 lon.: -59.431596 hgts: 500, 2000, 4000 m AMSL
Trajectory Direction: Backward Duration: 240 hrs
Vertical Motion Calculation Method: Model Vertical Velocity
Meteorology: 0000Z 8 Aug 2017 - GDAS1

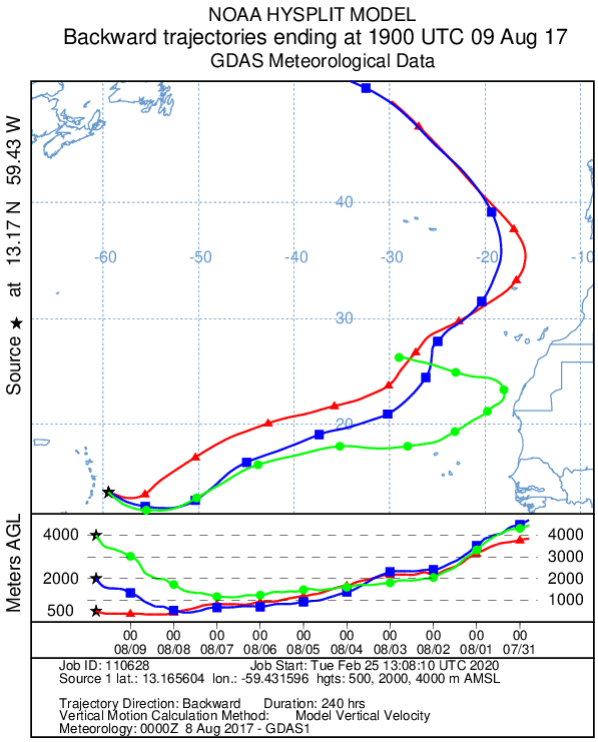
NOAA HYSPLIT MODEL
Backward trajectories ending at 1900 UTC 09 Aug 17
GDAS Meteorological Data
Source ★ at 13.17 N 59.43 W
Meters AGL
Job ID: 110628 Job Start: Tue Feb 25 13:08:10 UTC 2020
Source 1 lat.: 13.165604 lon.: -59.431596 hgts: 500, 2000, 4000 m AMSL
Trajectory Direction: Backward Duration: 240 hrs
Vertical Motion Calculation Method: Model Vertical Velocity
Meteorology: 0000Z 8 Aug 2017 - GDAS1

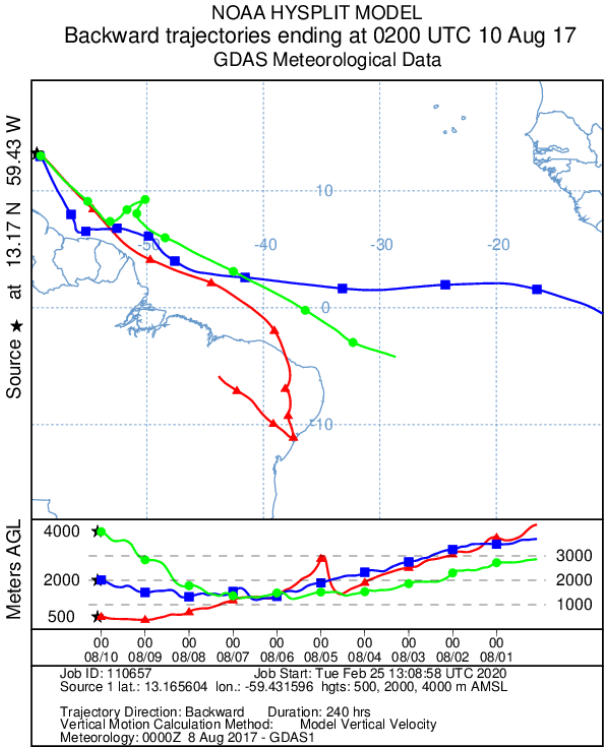
NOAA HYSPLIT MODEL
Backward trajectories ending at 0200 UTC 10 Aug 17
GDAS Meteorological Data
Source ★ at 13.17 N 59.43 W
Meters AGL
Job ID: 110657 Job Start: Tue Feb 25 13:08:58 UTC 2020
Source 1 lat.: 13.165604 lon.: -59.431596 hgts: 500, 2000, 4000 m AMSL
Trajectory Direction: Backward Duration: 240 hrs
Vertical Motion Calculation Method: Model Vertical Velocity
Meteorology: 0000Z 8 Aug 2017 - GDAS1

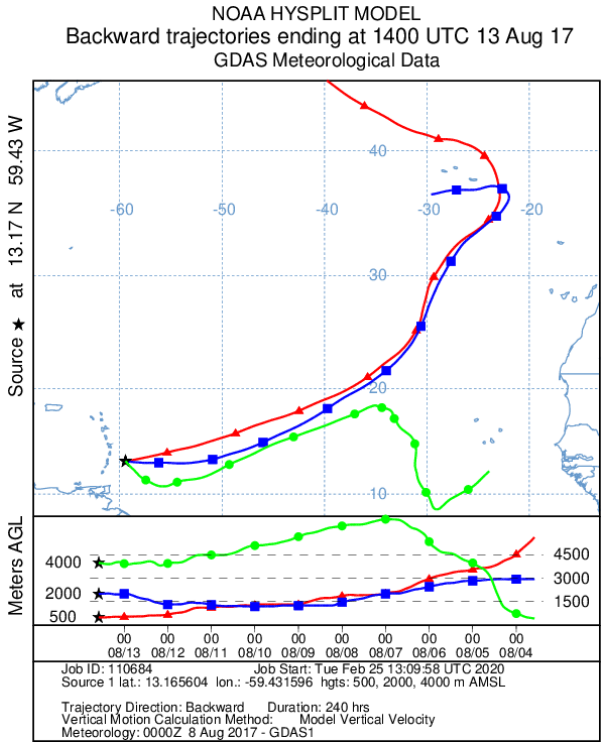
NOAA HYSPLIT MODEL
Backward trajectories ending at 1400 UTC 13 Aug 17
GDAS Meteorological Data
Source ★ at 13.17 N 59.43 W
Meters AGL
Job ID: 110684 Job Start: Tue Feb 25 13:09:58 UTC 2020
Source 1 lat.: 13.165604 lon.: -59.431596 hgts: 500, 2000, 4000 m AMSL
Trajectory Direction: Backward Duration: 240 hrs
Vertical Motion Calculation Method: Model Vertical Velocity
Meteorology: 0000Z 8 Aug 2017 - GDAS1

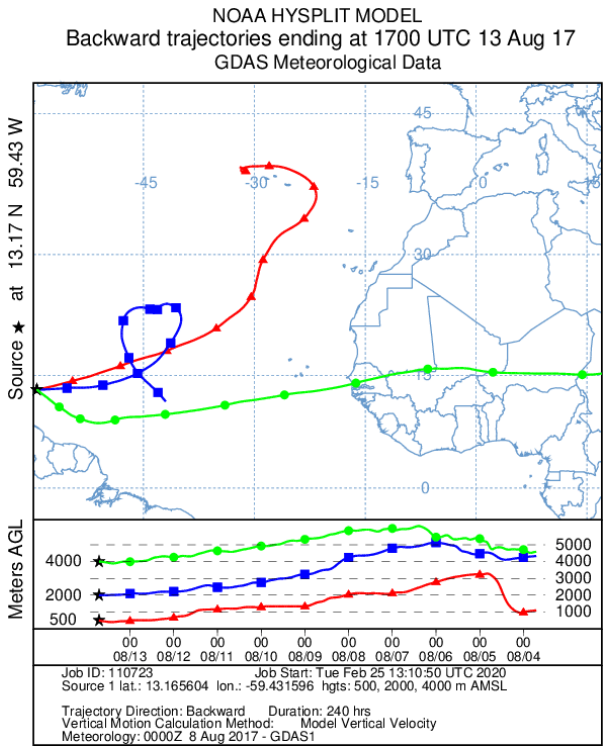
NOAA HYSPLIT MODEL
Backward trajectories ending at 1700 UTC 13 Aug 17
GDAS Meteorological Data
Source ★ at 13.17 N 59.43 W
Meters AGL
Job ID: 110723 Job Start: Tue Feb 25 13:10:50 UTC 2020
Source 1 lat.: 13.165604 lon.: -59.431596 hgts: 500, 2000, 4000 m AMSL
Trajectory Direction: Backward Duration: 240 hrs
Vertical Motion Calculation Method: Model Vertical Velocity
Meteorology: 0000Z 8 Aug 2017 - GDAS1

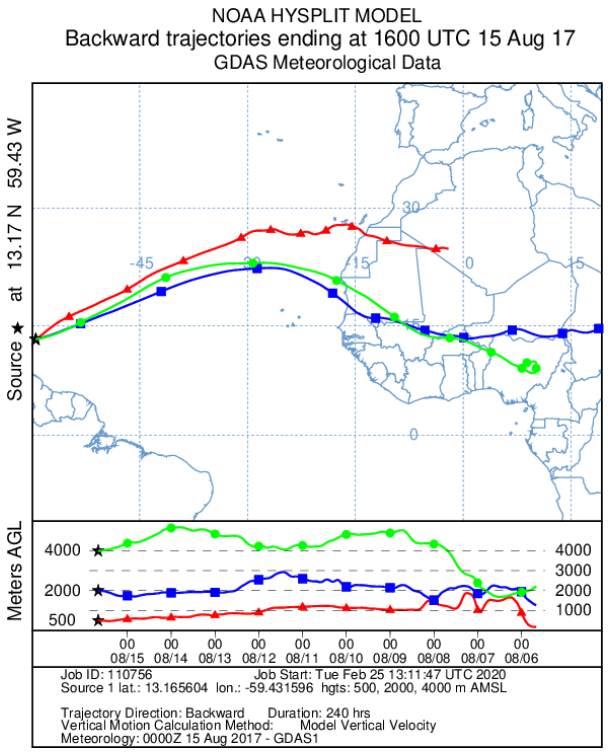
NOAA HYSPLIT MODEL
Backward trajectories ending at 1600 UTC 15 Aug 17
GDAS Meteorological Data
Source ★ at 13.17 N 59.43 W
Meters AGL
Job ID: 110756 Job Start: Tue Feb 25 13:11:47 UTC 2020
Source 1 lat.: 13.165604 lon.: -59.431596 hgts: 500, 2000, 4000 m AMSL
Trajectory Direction: Backward Duration: 240 hrs
Vertical Motion Calculation Method: Model Vertical Velocity
Meteorology: 0000Z 15 Aug 2017 - GDAS1

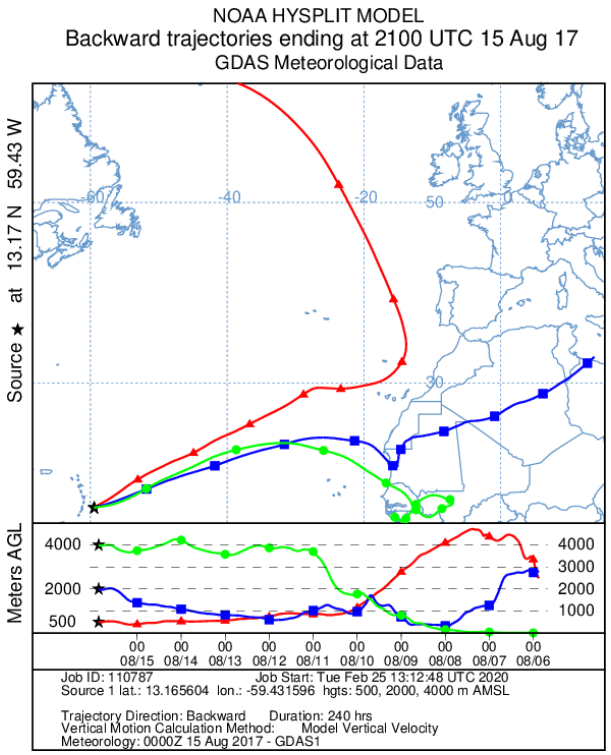
NOAA HYSPLIT MODEL
Backward trajectories ending at 2100 UTC 15 Aug 17
GDAS Meteorological Data
Source ★ at 13.17 N 59.43 W
Meters AGL
Job ID: 110787 Job Start: Tue Feb 25 13:12:48 UTC 2020
Source 1 lat.: 13.165604 lon.: -59.431596 hgts: 500, 2000, 4000 m AMSL
Trajectory Direction: Backward Duration: 240 hrs
Vertical Motion Calculation Method: Model Vertical Velocity
Meteorology: 0000Z 15 Aug 2017 - GDAS1

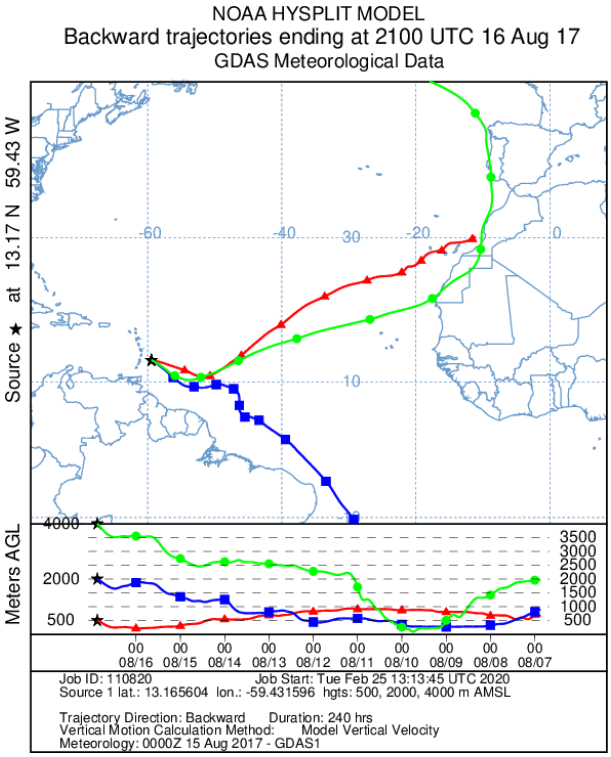
NOAA HYSPLIT MODEL
Backward trajectories ending at 2100 UTC 16 Aug 17
GDAS Meteorological Data
Source ★ at 13.17 N 59.43 W
Meters AGL
Job ID: 110820 Job Start: Tue Feb 25 13:13:45 UTC 2020
Source 1 lat.: 13.165604 lon.: -59.431596 hgts: 500, 2000, 4000 m AMSL
Trajectory Direction: Backward Duration: 240 hrs
Vertical Motion Calculation Method: Model Vertical Velocity
Meteorology: 0000Z 15 Aug 2017 - GDAS1

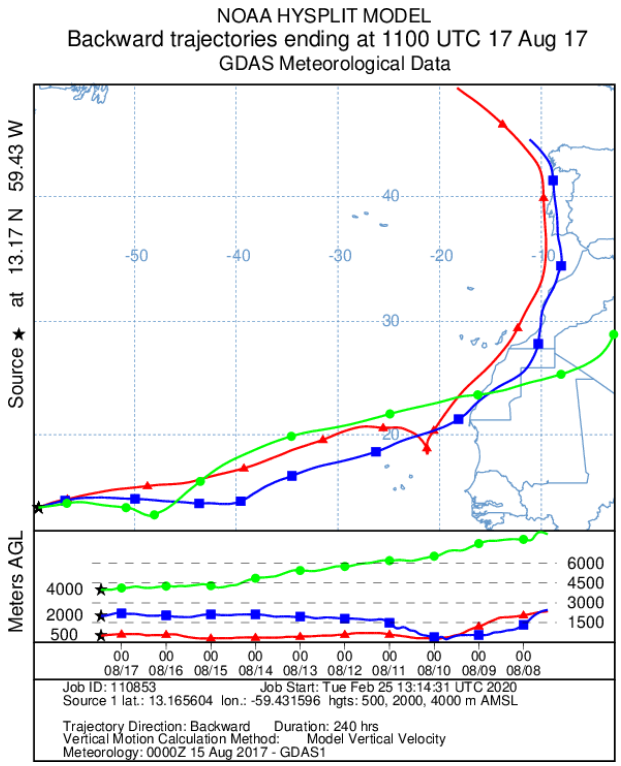
NOAA HYSPLIT MODEL
Backward trajectories ending at 1100 UTC 17 Aug 17
GDAS Meteorological Data
Source ★ at 13.17 N 59.43 W
Meters AGL
Job ID: 110853 Job Start: Tue Feb 25 13:14:31 UTC 2020
Source 1 lat.: 13.165604 lon.: -59.431596 hgts: 500, 2000, 4000 m AMSL
Trajectory Direction: Backward Duration: 240 hrs
Vertical Motion Calculation Method: Model Vertical Velocity
Meteorology: 0000Z 15 Aug 2017 - GDAS1

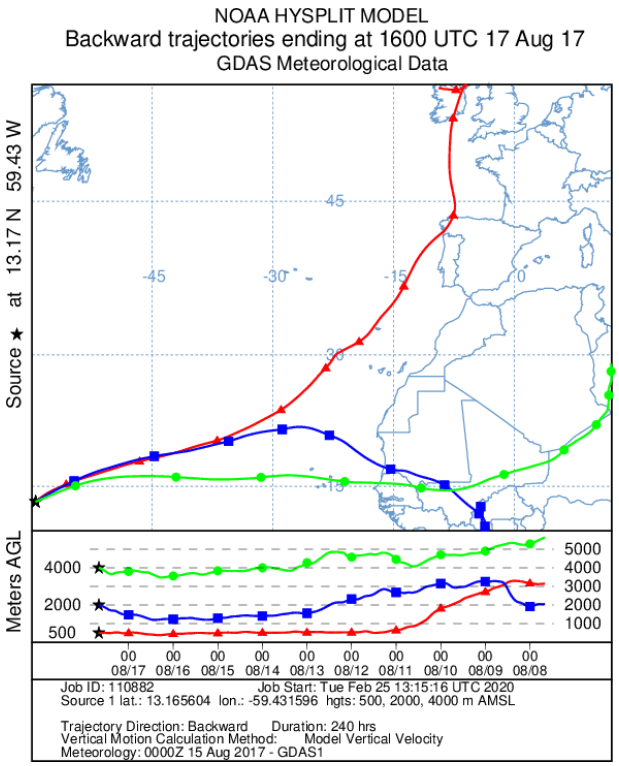
NOAA HYSPLIT MODEL
Backward trajectories ending at 1600 UTC 17 Aug 17
GDAS Meteorological Data
Source ★ at 13.17 N 59.43 W
Meters AGL
Job ID: 110882 Job Start: Tue Feb 25 13:15:16 UTC 2020
Source 1 lat.: 13.165604 lon.: -59.431596 hgts: 500, 2000, 4000 m AMSL
Trajectory Direction: Backward Duration: 240 hrs
Vertical Motion Calculation Method: Model Vertical Velocity
Meteorology: 0000Z 15 Aug 2017 - GDAS1

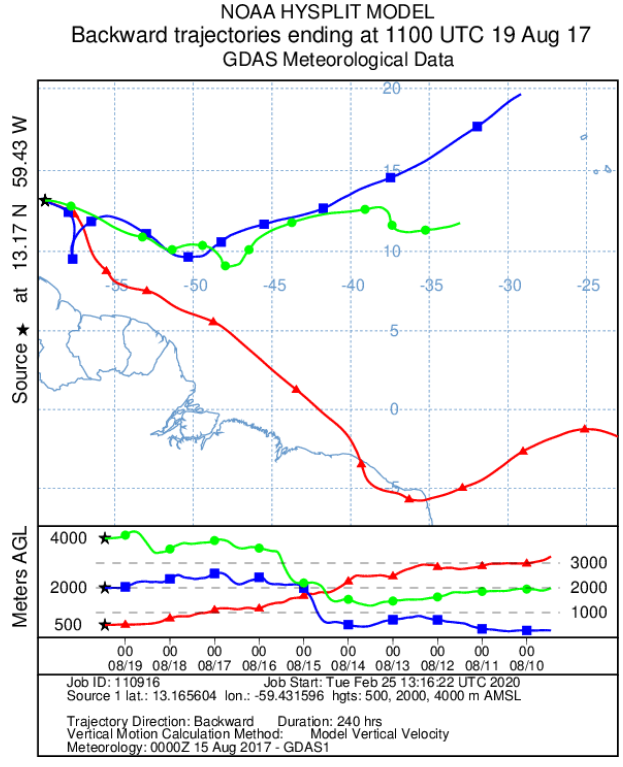
NOAA HYSPLIT MODEL
Backward trajectories ending at 1100 UTC 19 Aug 17
GDAS Meteorological Data
Source ★ at 13.17 N 59.43 W
Meters AGL
Job ID: 110916 Job Start: Tue Feb 25 13:16:22 UTC 2020
Source 1 lat.: 13.165604 lon.: -59.431596 hgts: 500, 2000, 4000 m AMSL
Trajectory Direction: Backward Duration: 240 hrs
Vertical Motion Calculation Method: Model Vertical Velocity
Meteorology: 0000Z 15 Aug 2017 - GDAS1

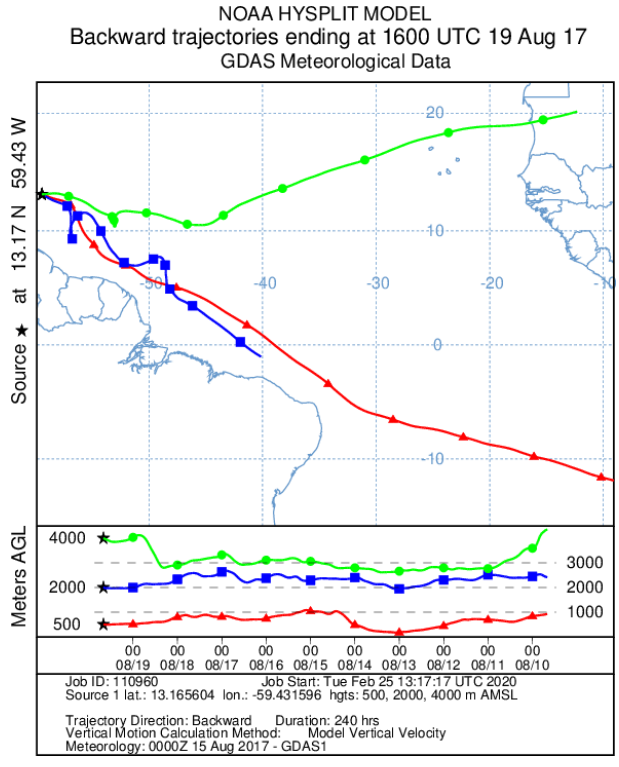
NOAA HYSPLIT MODEL
Backward trajectories ending at 1600 UTC 19 Aug 17
GDAS Meteorological Data
Source ★ at 13.17 N 59.43 W
Meters AGL
Job ID: 110960 Job Start: Tue Feb 25 13:17:17 UTC 2020
Source 1 lat.: 13.165604 lon.: -59.431596 hgts: 500, 2000, 4000 m AMSL
Trajectory Direction: Backward Duration: 240 hrs
Vertical Motion Calculation Method: Model Vertical Velocity
Meteorology: 0000Z 15 Aug 2017 - GDAS1

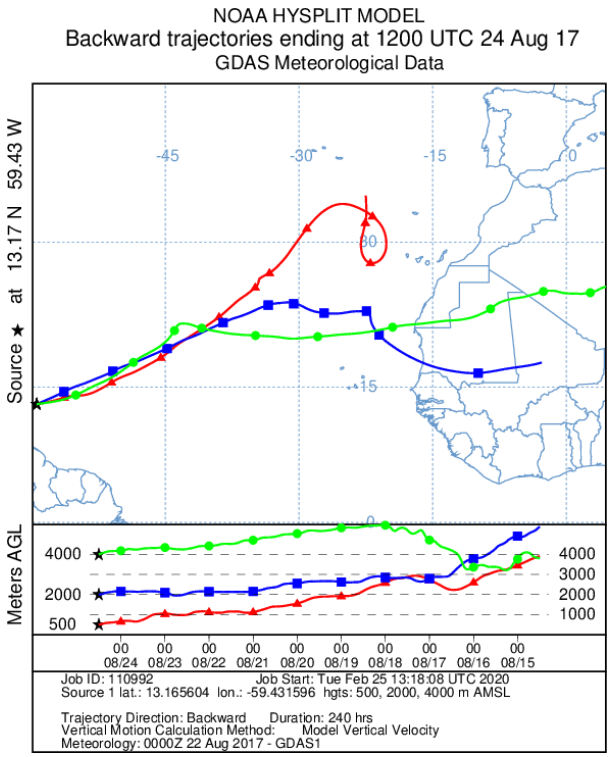

Figure S6: HYSPLIT ten day back trajectories (Stein et al., 2015) for the date and times of the filter samples collected in this study. Above ground level (AGL) altitudes of 500 m (shown in red), 2000 m (shown in green), and 4000 m (shown in blue) were chosen to represent the marine boundary layer and the base of the Saharan air layer (SAL) and top of the SAL. The star represents the starting location in Barbados.

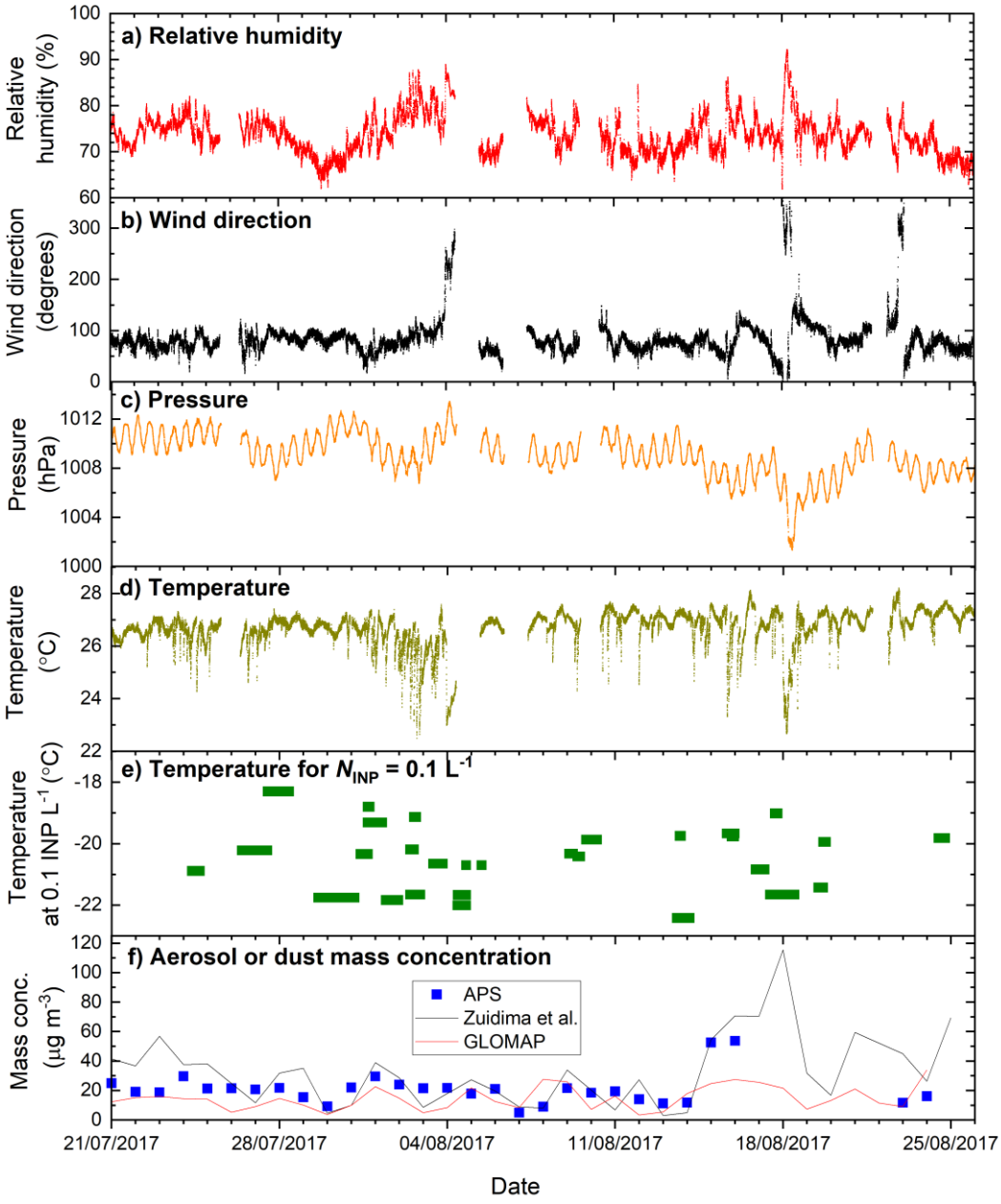

Figure S7: Time series for the (a) relative humidity, (b) wind direction, (c) pressure, (d) temperature, (e) N_{INP} at 0.1 L^{-1}, and (e) aerosol mass. The INP concentration of 0.1 L^{-1} was chosen to offer the greatest time resolution as most filter samples gave data points at this concentration. The dust mass concentration from Zuidema et al. (2019) is shown alongside that determined from our APS measurements.

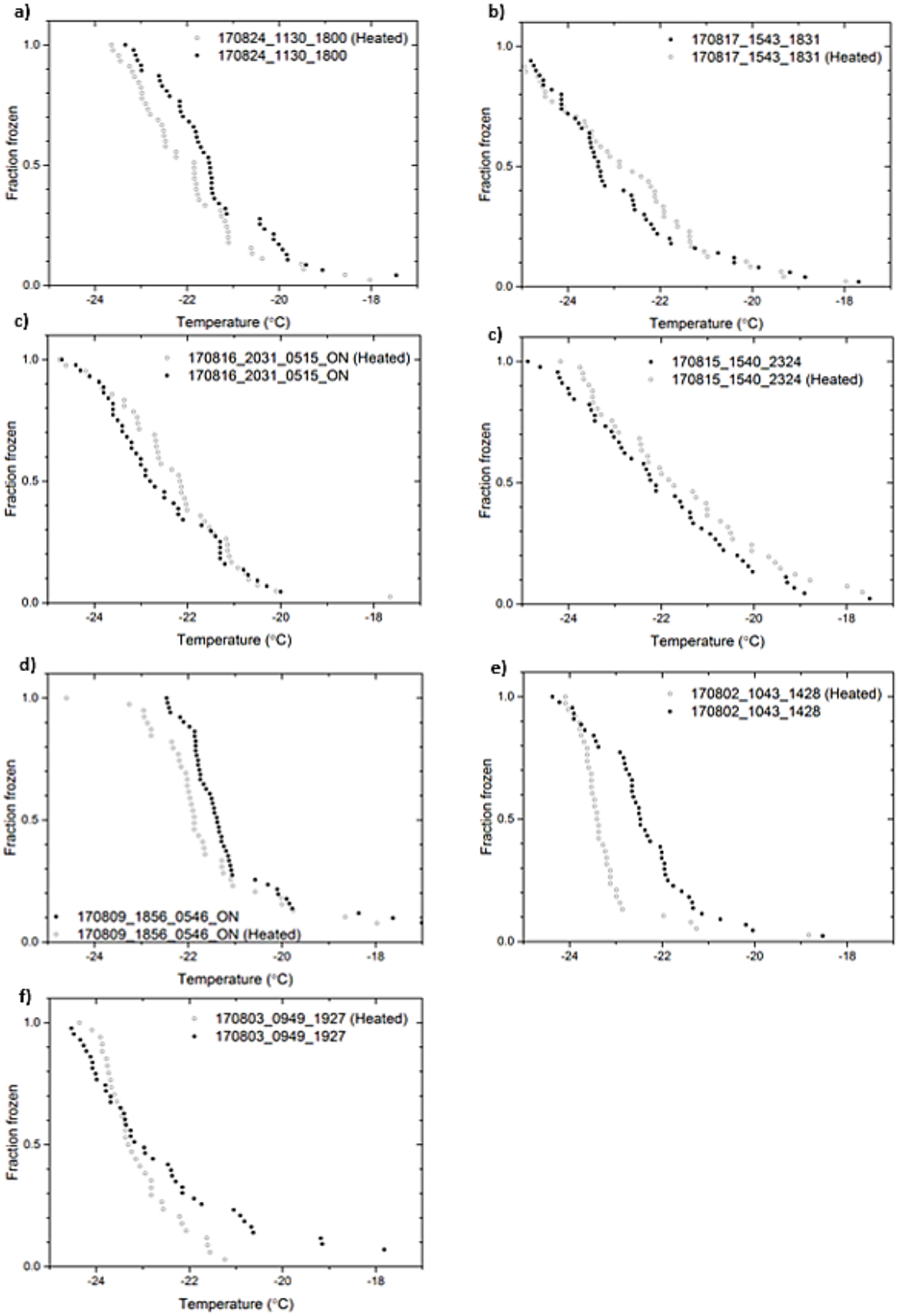

Figure S8: The fraction frozen curves for heated and unheated aerosol suspensions. a-f) Fraction frozen curves for aerosol suspensions before and after heat treatment. Also see Figure 6 in the main paper.

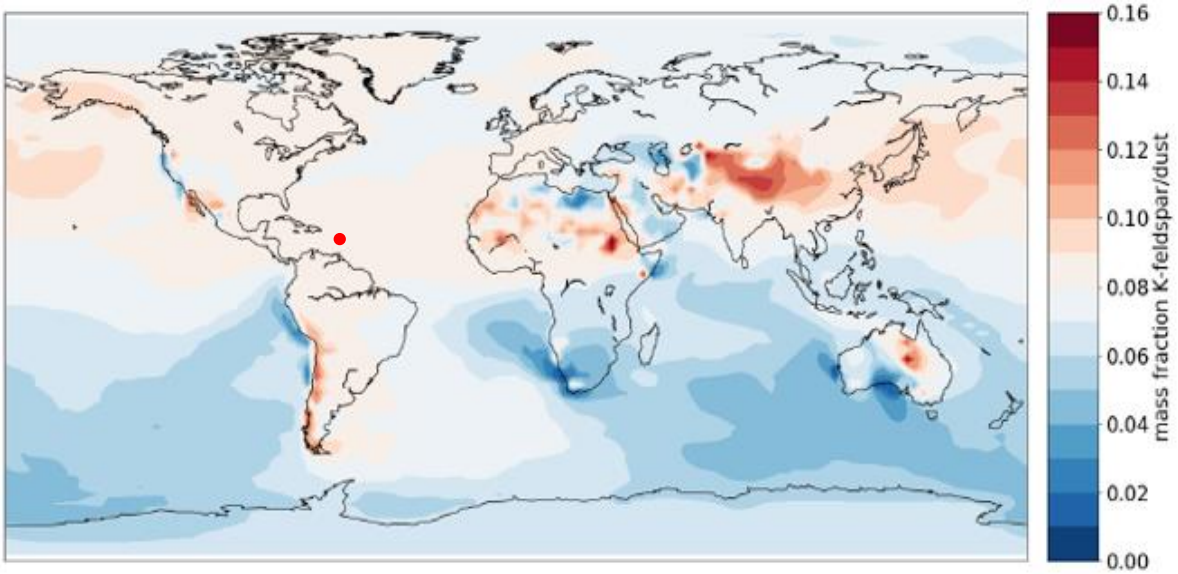

Figure S9: GLOMAP model simulation of the mass fraction of K-feldspar relative to aerosolised mineral dust at the surface. In Barbados, it can be seen that K-feldspar is predicted to account for roughly 8 % of the aerosolised mineral dust (rather than the 0.1-2% that was measured). The red point marks the location of Barbados.

References

Harrison, A. D., Lever, K., Sanchez-Marroquin, A., Holden, M. A., Whale, T. F., Tarn, M. D., McQuaid, J. B., and Murray, B. J.: The ice-nucleating ability of quartz immersed in water and its atmospheric importance compared to K-feldspar, Atmos. Chem. Phys., 19, 11343-11361, 10.5194/acp-19-11343-2019, 2019.

Stein, A. F., Draxler, R. R., Rolph, G. D., Stunder, B. J. B., Cohen, M. D., and Ngan, F.: NOAA?s HYSPLIT Atmospheric Transport and Dispersion Modeling System %J Bulletin of the American Meteorological Society, 96, 2059-2077, 10.1175/bams-d-14-00110.1, 2015.

Vali, G.: Revisiting the differential freezing nucleus spectra derived from drop-freezing experiments: methods of calculation, applications, and confidence limits, Atmos. Meas. Tech., 12, 1219-1231, 10.5194/amt-12-1219-2019, 2019.

Whale, T. F., Murray, B. J., O'Sullivan, D., Wilson, T. W., Umo, N. S., Baustian, K. J., Atkinson, J. D., Workneh, D. A., and Morris, G. J.: A technique for quantifying heterogeneous ice nucleation in microlitre supercooled water droplets, Atmos. Meas. Tech., 8, 2437-2447, 10.5194/amt-8-2437-2015, 2015.

Zuidema, P., Alvarez, C., Kramer, S. J., Custals, L., Izaguirre, M., Sealy, P., Prospero, J. M., and Blades, E.: Is Summer African Dust Arriving Earlier to Barbados? The Updated Long-Term In Situ Dust Mass

Concentration Time Series from Ragged Point, Barbados, and Miami, Florida, Bulletin of the American Meteorological Society, 100, 1981-1986, 10.1175/bams-d-18-0083.1, 2019.